Alexandria Engineering Journal 97 (2024) 376–384

Contents lists available at ScienceDirect

Alexandria Engineering Journal

journal homepage: www.elsevier.com/locate/aej

Original Article

Oscillator without equilibrium and linear terms: Dynamics and application

Victor Kamdoum Tamba [a], Viet-Thanh Pham [b,*], Ali A. Shukur [c], Giuseppe Grassi [d,*], Saher Momani [e,f]

[a] Department of Telecommunication and Network Engineering, IUT-Fotso Victor of Bandjoun, University of Dschang, Bandjoun, P. O. Box: 134, Cameroon
[b] Faculty of Electronics Technology, Industrial University of Ho Chi Minh City, Ho Chi Minh City, Vietnam
[c] Faculty of Computer Sciences and Mathematics, University of Kufa, An-Najaf, Iraq
[d] Department of Engineering for Innovation, University of Salento, Lecce, 73100, Italy
[e] Nonlinear Dynamics Research Center (NDRC), Ajman University, Ajman, 20550, United Arab Emirates
[f] Department of Mathematics, Faculty of Science, University of Jordan, Amman, 11942, Jordan

ARTICLE INFO

MSC:
37M05
37N35
65P20

Keywords:
Chaotic system
Hidden attractor
Microcontroller
Equilibrium
Encryption

ABSTRACT

A significant attention has concentrated on systems with “hidden attractors” in recent years. The aim of this work is to study an oscillator displaying “hidden attractors”. The oscillator has all nonlinear terms but no equilibrium. The oscillator exhibits attractive dynamics such as chaos, bubble bifurcation, symmetrical attractors, and boosting attractors. Oscillator’s feasibility is verified by a microcontroller. Utilizing the oscillator for biomedical image encryption illustrates its application. In addition, the adaptive control is designed for the oscillator.

1. Introduction

The chaotic oscillator is one of the attractive areas of applied sciences. According to most acceptable definition, it is a nonlinear dynamical system having a characteristic that is sensitive to initial conditions. Chaotic oscillators are used in many scientific and engineering fields, including communications, due to their complicated and unexpected behavior [1], neural networks [2], image encryption [3], robotics [4], pattern recognition [5], and biomedical applications [6].

Due to the above brief introduction, in the past twenty years, scientists, engineers, and mathematicians have been increasingly interested in the studies of chaotic oscillators and their applications. Hence, after the discovery of Lorenz’s three-dimensional system in 1963 [7], researchers have attempted to present chaotic oscillators with unique features. Chaotic oscillators without equilibrium were reported in [8,9]. Chaotic oscillators with stable equilibrium were presented in [10–12] while chaotic oscillators with equilibrium point lies on a segmented straight line were studied in [13–16]. Moreover, chaotic oscillators with curve of equilibria and circular equilibrium were presented in [17] and [18], respectively.

Around the basin of attraction, each dynamic system has different kind of attractors such as: periodic attractors, a quasi-periodic and strange attractor. The basin is connected with an attractor contains all the initial conditions of the space. As time moves towards infinity, the orbits of these conditions change the attractor and move closer to it. Nowadays, by the discovery of “hidden attractors” in [19] whose basins do not touch (or contain) a small neighborhood of any equilibrium points, chaotic attractor can be classified as either hidden attractor or a self-exited.

Moreover, providing new chaotic oscillators with special properties is among the most significant obstacles facing many scholars. Chaotic oscillators can be divided into conservative, dissipative and peculiar categories. A dissipative chaotic system is one in which energy or other stored quantities are continually lost and, for instance, often converted to heat by processes such as friction [20]. The behavior of the system may be unpredictable and limited to the boundaries of these attrac-

* Corresponding authors.
E-mail addresses: phamvietthanh@iuh.edu.vn (V.-T. Pham), giuseppe.grassi@unisalento.it (G. Grassi).

https://doi.org/10.1016/j.aej.2024.04.029
Received 11 February 2024; Received in revised form 2 April 2024; Accepted 14 April 2024
Available online 30 April 2024

tors, vice versa, conservative chaotic oscillators do not loss energy over time. Their orbits appear on the surface exhibiting constant energy in phase space. Despite their chaotic nature, the orbits of these oscillators remain within conserved boundaries. Recently, there are peculiar chaotic oscillators that do not precisely fit within conservative or dissipative categories. This kind of high complicated oscillators can interact with both. It operates according to principles of conservation and dissipation of energy, or defies traditional classification. Their behavior is particularly fascinating and provides insight into the diversity of chaos in different environments. Conservative and dissipative chaotic oscillators are structurally stable. However, the initial conditions fall within the chaotic basin or not, the orbits of such oscillators whether chaotic or not are bounded. On the other hand, the behavior of a peculiar chaotic may change suddenly. Depending on its conditions, it can respond with either bounded or unbounded oscillation. Therefore, designing and studying such peculiar oscillators is a very hard task. For example, having a positive, zero and negative Lyapunov exponents of three dimensional autonomous chaotic oscillator with unstable equilibrium points, the boundedness of its orbits under all possible initial conditions does not necessarily guarantee. Consequently, the basin of attraction is an essential tool that should be used to recognize the chaotic and other dynamics, particularly, for peculiar chaotic dynamics.

In the present paper, we introduce a chaotic oscillator with only pure nonlinear terms. The oscillator exhibits hidden attractors. Despite of absence of equilibrium, the oscillator displays special dynamics such as chaos, bubble bifurcation, symmetrical and boosting attractors. Feasibility, application, and adaptive controller of the oscillator are investigated. The novelty and significance of our findings contribute to the field of nonlinear dynamics and its applications. The organization of this paper is as the following: in section 2, we present a chaotic oscillator with only pure nonlinear terms (cubic and signum) where the proposed oscillator has no equilibrium points. Bifurcation diagrams, and Lyapunov exponents have all been used to examine the proposed oscillator. In section 3, we present a microcontroller implementation of the proposed oscillator offers many advantages such as high calculation speed, high stability and precision, great flexibility and the possibility to modify the system parameters and initial conditions easily. In sections 4 and 5, we design an algorithm for encryption of biomedical images. The main steps of applying the proposed oscillator to biomedical image encryption (and decryption) are described. The resilience of the proposed algorithm for biological image encryption gets evaluated. In section 6, we report the adaptive control of the oscillator.

2. Model and dynamics of the oscillator

Cubic and signum functions are common elements for designing chaotic oscillator. Based on such terms, we propose an oscillator without linear terms as follows:

$$\begin{cases} \dot{x} = a\left(z^3 - \operatorname{sgn}(y)\right), \\ \dot{y} = -z^3 - b, \\ \dot{z} = -z^3 - x^3, \end{cases} \tag{1}$$

here a, and b are parameters. We find the equilibrium of (1) by solving:

$$a\left(z^3 - \operatorname{sgn}(y)\right) = 0, \tag{2}$$

$$-z^3 - b = 0, \tag{3}$$

$$-z^3 - x^3 = 0. \tag{4}$$

From Eqs. (2), (3) we get

$$\operatorname{sgn}(y) = -b. \tag{5}$$

As a result, the oscillator has no equilibrium when $b \neq 0, \pm 1$. We focus on the case in which there is no equilibrium in the oscillator.

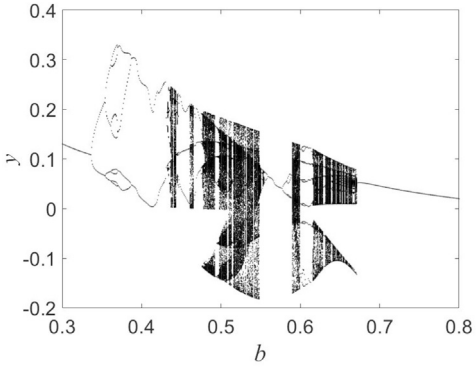

Fig. 1. Bifurcation diagram when varying b.

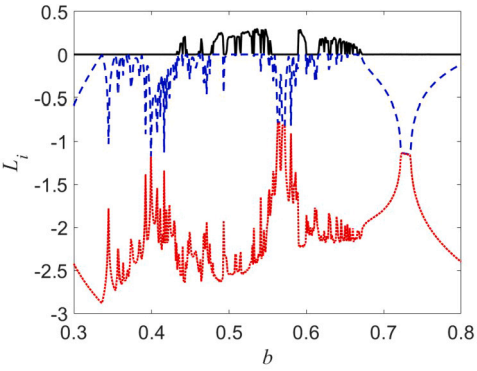

Fig. 2. Lyapunov exponents of the system.

By keeping $a = 3$ and changing b, dynamics of the oscillator is shown in Fig. 1 and Fig. 2. Here initial conditions are equal to zero. Bubble bifurcation is observed in the range $b \in [0.3, 0.4]$, see Fig. 1. The oscillator displays chaos and periodical signals. Chaos is illustrated in Fig. 3 for $a = 3$ and $b = 0.5$. The Lyapunov exponents are found to be $L_1 = 0.2054$, $L_2 = 0$, $L_3 = -2.5459$. Therefore, the Kaplan–Yorke dimension is $D_{KY} = 2.0807$, indicating that the Lyapunov dimension is fractional.

From Eq. (1), we see that the oscillator is not changed via the transformation $(x, y, z, b) \leftrightarrow (-x, -y, -z, -b)$. System displays symmetric attractors when changing the polarity of b as illustrated in Fig. 4.

Theorem 1. *The oscillator (1) is dissipative for $z(t) > 0$ or $z(t) < 0$ as $t \to \infty$.*

Proof. The divergence of vector field is given by:

$$V = \frac{\partial \dot{x}}{\partial x} + \frac{\partial \dot{y}}{\partial y} + \frac{\partial \dot{z}}{\partial z} = -3z^2. \tag{6}$$

From Eq. (6), one can see that the proposed oscillator (1) is dissipative for $z(t) > 0$ or $z(t) < 0$ as $t \to \infty$.

The study of the dynamical behavior of a system is very interesting when we vary simultaneously at least two of its parameters. This allows to examine its global behavior. Fig. 5 shows the 2D bifurcation diagram of our oscillator by simultaneously varying the parameters a and b. By setting zero initial conditions, one can observe that the oscillator's dynamics changes when a and b are varied simultaneously. The choice of the values of a and b in the green zones leads to periodic behaviors. While, these values selected in the blue areas give chaotic behaviors.

We can introduce three control parameters into the oscillator in the form:

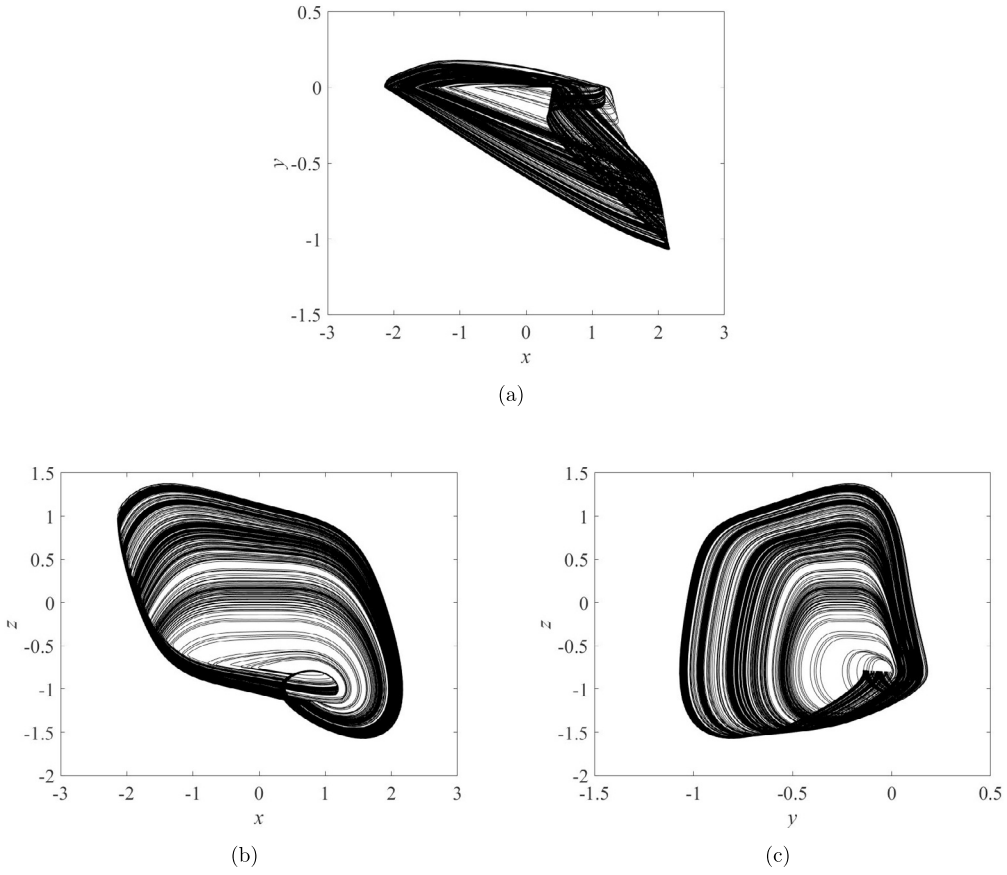

Fig. 3. Phase portraits of system (1) in (a) $x-y$, (b) $x-z$, and (c) $y-z$ for $a=3$, $b=0.5$.

$$\begin{cases} \dot{x} = a\left(\left(z+k_z\right)^3 - \operatorname{sgn}\left(y+k_y\right)\right), \\ \dot{y} = -\left(z+k_z\right)^3 - b, \\ \dot{z} = -\left(z+k_z\right)^3 - \left(x+k_x\right)^3, \end{cases} \tag{7}$$

for boosting the oscillator's attractors.

3. Microcontroller implementation of no equilibrium oscillator

Today, microcontrollers are currently used to easily implement chaotic oscillators. Compared to electronic circuit implementation, this method offers many advantages such as high calculation speed, high stability and precision, great flexibility and the possibility to modify the system parameters and initial conditions easily. For these reasons, in this paper the no equilibrium oscillator is implemented by using Arduino Due microcontroller. This card has the advantage of having an integrated digital to analog converter, which facilitates the implementation. The experimental results are observed and captured by using a dual-channel digital oscilloscope (Voltcraft D50-1062D). The fourth-order Runge-Kutta algorithm is used to discretize the no equilibrium oscillator with the discretization step equal to 0.001. Using the same values of system parameters and initial conditions ($a=3$, $b=0.5$ and $x(0)=y(0)=z(0)=0$) keeping in Fig. 3, we display the corresponding experimental chaotic phase diagrams in Fig. 6. One can notice that the numerical and experimental results agree. This confirms that Arduino Due microcontroller successfully implements the dynamics of the no equilibrium oscillator.

4. Design of an algorithm for encoding biomedical image

Here, we exploit the attractive behaviors of the oscillator without equilibrium and linear term to design an algorithm for encoding biomedical image. The efficiency of the elaborated algorithm is verified by performing some performance tests.

4.1. Description of the biomedical image encryption

The biomedical image encryption process based on the proposed three-dimensional chaotic system is presented in Fig. 7.

Five main steps below describe the encoding algorithm:

Step 1: The oscillator without equilibrium and linear term is integrated with Runge Kutta method. It is sufficiently pre-iterated to eliminate the transitional phase. This operation improves the algorithm's performance. The system is now iterated 256×256 times and its state variables (x, y and z) are extracted after each iteration to construct the secret keys $K_1(i)$ and $K_2(i)$ below:

$$K_1(i) = \left(x_i + y_i + z_i + 10\right)/2 \tag{8}$$

$$K_2(i) = \operatorname{mod}\left(round\left(\left(x_i + y_i + z_i\right)\times10^{15}\right), 256\right) \tag{9}$$

Step 2: The initial image undergoes a diffusion based on the mirror effect given by the following equation

$$M(k) = \begin{cases} I(i,j) & \text{if} \quad \operatorname{mod}(i,2)=0 \text{ with } S_c \geq j \geq 1 \text{ and } 1 \leq i \leq S_r \\ I(i,j) & \text{if} \quad \operatorname{mod}(i,2)\neq 0 \text{ with } 1 \leq j \leq S_c \text{ and } 1 \leq i \leq S_r \end{cases} \tag{10}$$

Thus, the resulting diffused image $M(i)$ is obtained.

Step 3: The diffused image $M(i)$ and secret key $K_1(i)$ are applied to a permutation module to obtain the permutated image $P(i)$.

Step 4: The permutated image $P(i)$ is introduced in the confusion layer based on the S-Box and then the confused image $B(i)$ is produced.

Step 5: The confused image $B(i)$ and secret key $K_2(i)$ are then mixed in the last block to create the encoded image. The decoding process is carried out by all the reverse encoding operations.

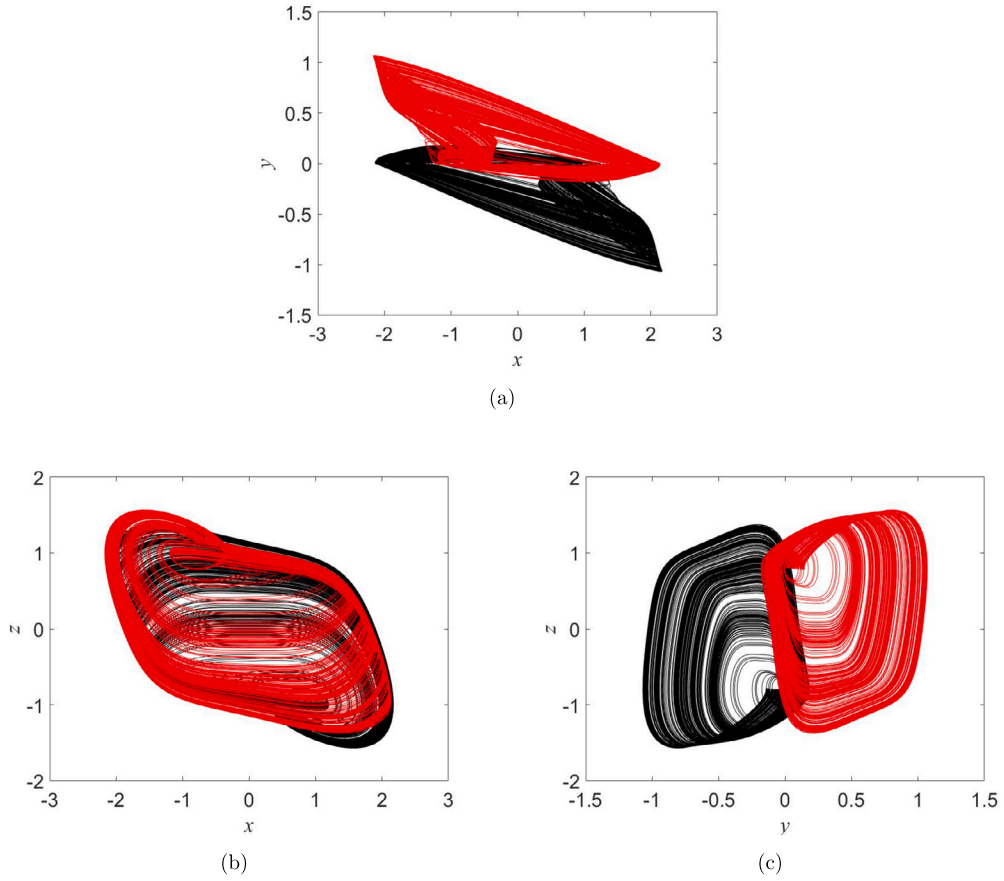

Fig. 4. Phase portraits of oscillator (1) in (a) $x-y$, (b) $x-z$, and (c) $y-z$ for $a=3$, $b=0.5$ (black), and $b=-0.5$ (red).

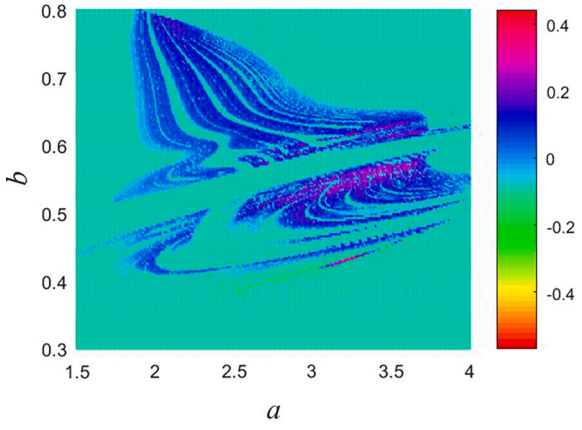

Fig. 5. 2D bifurcation diagram of system showing its global dynamical behavior for the parameters a and b varying simultaneously.

4.2. Simulations results of the elaborated scheme for encoding biomedical image

All the simulations are computed in MATLAB 2016b. In this work, we use three gray-scale biomedical images of size 256×256, namely glioma, meningioma and pituitary. These are images of brain diseases. According to the encoding and decoding procedures described below, the encoded and decoded biomedical images are shown in Fig. 8.

From Fig. 8, it is clear that the initial images are very different from those that have been encoded. This demonstrates the effectiveness of the elaborated encoding scheme.

Table 1
Information entropies of initial and encoded biomedical images.

	Images		
Entropy	Glioma	Meningioma	Pituitary
Initial image	5.3328	5.5266	5.7618
Encoded image	7.9970	7.9973	7.9975

5. Algorithm performance tests

5.1. Information entropy

The information entropy is expressed as [21]

$$H(m) = -\sum_{i=1}^{N} P(m_i) \log_2 (m_i), \tag{11}$$

in which N and $P(m_i)$ represent respectively, the total number and the probability of appearance of symbol m_i. According to (11), we provided the information entropy in Table 1.

The results in Table 1 show that the encoded images have entropy approaching 8, which is a standard value for a good encoding system. This confirms the robustness of the elaborated encoding system.

5.2. Correlation study

Let's consider another tool used to evaluate the performance of an encoding system which is the correlation coefficient (in short, CC). It expresses the rate of similarity between two neighboring pixels in an image [22]. The CC of initial image is close to 1 for initial image and tends to 0 for encoded image which is given by:

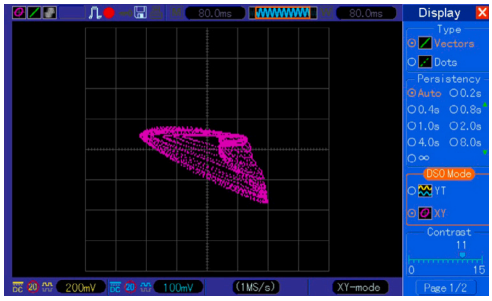

(a)

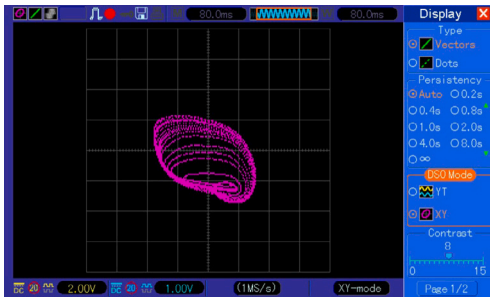

(b)

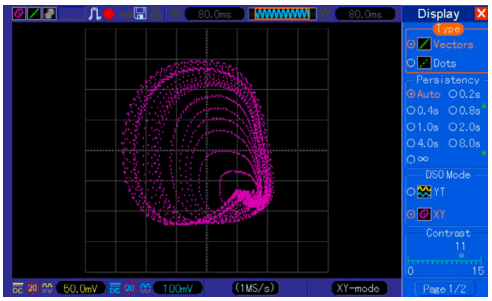

(c)

Fig. 6. The experimental chaotic phase diagrams observed and captured by using a dual-channel digital oscilloscope (Voltcraft D50-1062D): (a) $V_x - V_y$, (b) $V_x - V_z$, and (c) $V_y - V_z$.

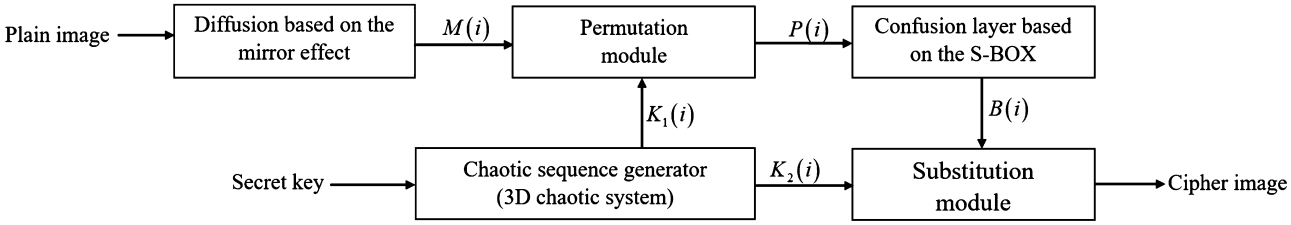

Fig. 7. Biomedical image encoding process based on the constructed oscillator without equilibrium and linear term.

Table 2
Correlation coefficients values computed in different directions.

Direction	Gray-scale images					
	Original image			Encrypted image		
	glioma	meningioma	pituitary	glioma	meningioma	pituitary
Horizontal	0.9531	0.9409	0.9407	0.00094	-0.0014	0.0010
Vertical	0.9539	0.9593	0.9336	-0.0032	-0.0013	0.0008
Diagonal	0.9242	0.9112	0.8890	-0.0020	-0.0028	-0.0010
Average	0.9437	0.9371	0.9211	-0.0014	-0.0018	0.00026

$$\begin{cases} E(x) = \frac{1}{N}\sum_{i=1}^{N} x_i \\ D(x) = \frac{1}{N}\sum_{i=1}^{N} \left(x_i - E(x)\right)^2 \\ \mathrm{cov}(x,y) = \frac{1}{N}\sum_{i=1}^{N} \left(x_i - E(x)\right)\left(y_i - E(y)\right) \\ r_{xy} = \frac{\mathrm{cov}(x,y)}{\sqrt{D(x)}\sqrt{D(y)}} \end{cases} \tag{12}$$

in which, x and y represent the pixel values. The results of correlation coefficients computed with the help of Eq. (12) are shown in Table 2.

The results in Table 2 show that the correlation coefficient values for initial images are close to 1. However, after encoding process, their values are all close to 0.

5.3. Histogram study

The histogram is used to appreciate the graphic distribution of pixels of an image. The pixels of an initial image are arranged randomly and those of encoded image are disposed uniformly. The histogram of the initial and encoded biomedical images is shown in Fig. 9.

We can observe from Fig. 9 that, the histogram of the initial, encoded and decoded biomedical images has the properties as described above. This proves that the elaborated encoding system is efficient.

5.4. Key space and key sensitivity evaluation

To ensure a good level of security in an encoding system, the required key space must exceed 2^{100}, see [23]. The investigated oscillator

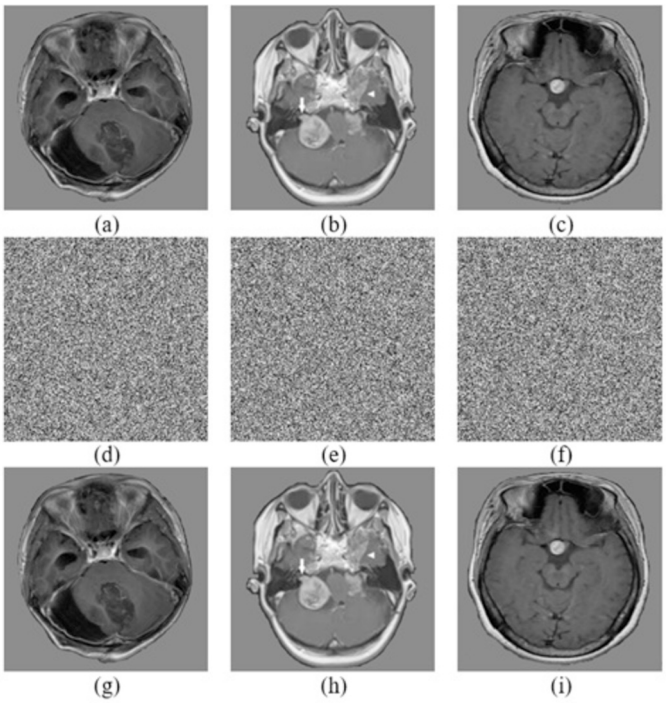

Fig. 8. Simulations results of the elaborated scheme for encoding biomedical image (a) initial image of glioma, (b) initial image of meningioma, (c) initial image of pituitary, (d) encoded image of glioma, (e) encoded image of meningioma, (f) encoded image of pituitary, (g) decoded image of glioma, (h) decoded image of meningioma, (i) decoded image of pituitary.

without equilibrium and linear term includes three initial states and two constant parameters. Considering a precision of 10^{-17}, the key space size is $10^{17\times5} = 10^{85}$, which exceeds 2^{100}. An algorithm for encoding image that is highly sensitive to the key has good resistance to brute force attacks. To evaluate the key sensitivity of the elaborated biomedical image-encoding algorithm, we use six slightly different test keys to decode the sending image, see Fig. 10.

From Fig. 10, we can realize that, a small change (10^{-17}) in the key has a large influence on the decoded image. In fact, when the key is slightly modified, it is no longer possible to receive the initial image. In conclusion, the elaborated encoding system has good sensitivity to the key.

5.5. Effects of noise and occlusion attacks

The encoding systems are sensitive to noise and occlusion attacks. It is therefore important to evaluate their effects on the performances of the encoding system. To this end, two types of noise (Gaussian, Salt and Pepper noise) are added to the initial biomedical images before the encoding process. The decoded images are shown in Fig. 11($a_1' - a_3'$) for Gaussian noise and Fig. 11($b_1' - b_3'$) for Salt and Pepper noise. In addition, a portion of the initial biomedical images (see Fig. 11($c_1 - c_3$) is removed before the encoding process. Fig. 11($c_1' - c_3'$) shows decoded images. From Fig. 11, one can see that, despite the addition of noise and the suppression of a portion of the initial images, the decoded images are still usable.

5.6. Effects of the differential attacks

The differential attacks influence the efficiency of an encoding system. The effects of differential attacks on an encoding system are examined using different tests such as NPCR and UACI. The mathematical expressions of NPCR and UACI are [24]:

Table 3
Results of the NPCR and UACI tests.

	Plaintext sensitivity	
Image	NPCR (%)	UACI (%)
glioma	99.5986	29.3736
Meningioma	99.6185	27.4038
Pituitary	99.5804	29.0642

$$NPCR = \frac{\sum_{i=1}^{m}\sum_{j=1}^{n} d(i,j)}{m\times n}\times 100 \tag{13}$$

$$d(i,j) = \begin{cases} 0, & if \quad p(i,j) = p'(i,j); \\ 1, & else, \end{cases}$$

and

$$UACI = \frac{100}{m\times n}\sum_{i=1}^{m}\sum_{j=1}^{n}\frac{|p(i,j) - p'(i,j)|}{2^{l}-1}. \tag{14}$$

According to Equations (13) and (14), the NPCR and UACI are evaluated and the results are listed in Table 3.

The results in Table 3 show that the elaborated encoding system is sensitive to small modifications to the image pixels.

5.7. Comparison of the results with those of some recent studies

Table 4 compares the results of this work with those developed in some recent studies [25–28].

The results in Table 4 clearly show that the encoding method developed in this work is efficient and resistant to different attacks than ones studied in some recent works.

6. Adaptive control of the oscillator

Control and synchronization are vital for chaotic systems [29–31]. Baleanu et al. studied state-feedback and optimal controllers for a quarter-car model [29]. State-feedback and adaptive controllers were proposed by Sajjadi et al. for a biological oscillator [30]. In [31], authors developed active and adaptive schemes for a cardiac conduction system. This section presents an adaptive controller of the oscillator.

Let define the driver system by

$$\begin{cases} \dot{x}_1 = a\left(x_3^3 - \mathrm{sgn}\left(x_2\right)\right), \\ \dot{x}_2 = -x_3^3 - b, \\ \dot{x}_3 = -x_3^3 - x_1^3. \end{cases} \tag{15}$$

In the next, we provide the adaptive synchronization of identical novel chaotic oscillator with parameters which are not valued. The response system is presented as

$$\begin{cases} \dot{x}_1 = ax_3^3 - a\mathrm{sgn}\left(x_2\right) + u_1, \\ \dot{x}_2 = -x_3^3 - b + u_2, \\ \dot{x}_3 = -x_3^3 - x_1^3 + u_3, \end{cases} \tag{16}$$

where x_1, x_2, x_3 are the states, a, b are unknown system parameters and

$U = [u_1, u_2, u_3]^T$

is the adaptive controller to be determined. We consider the adaptive controller defined by

$$\begin{cases} u_1 = -\varepsilon_a x_3^3 + \varepsilon_a \mathrm{sgn}\left(x_2\right) - x_1 k_1, \\ u_2 = x_3^3 + \varepsilon_b - x_2 k_2, \\ u_3 = x_3^3 + x_1^3 - x_3 k_3, \end{cases} \tag{17}$$

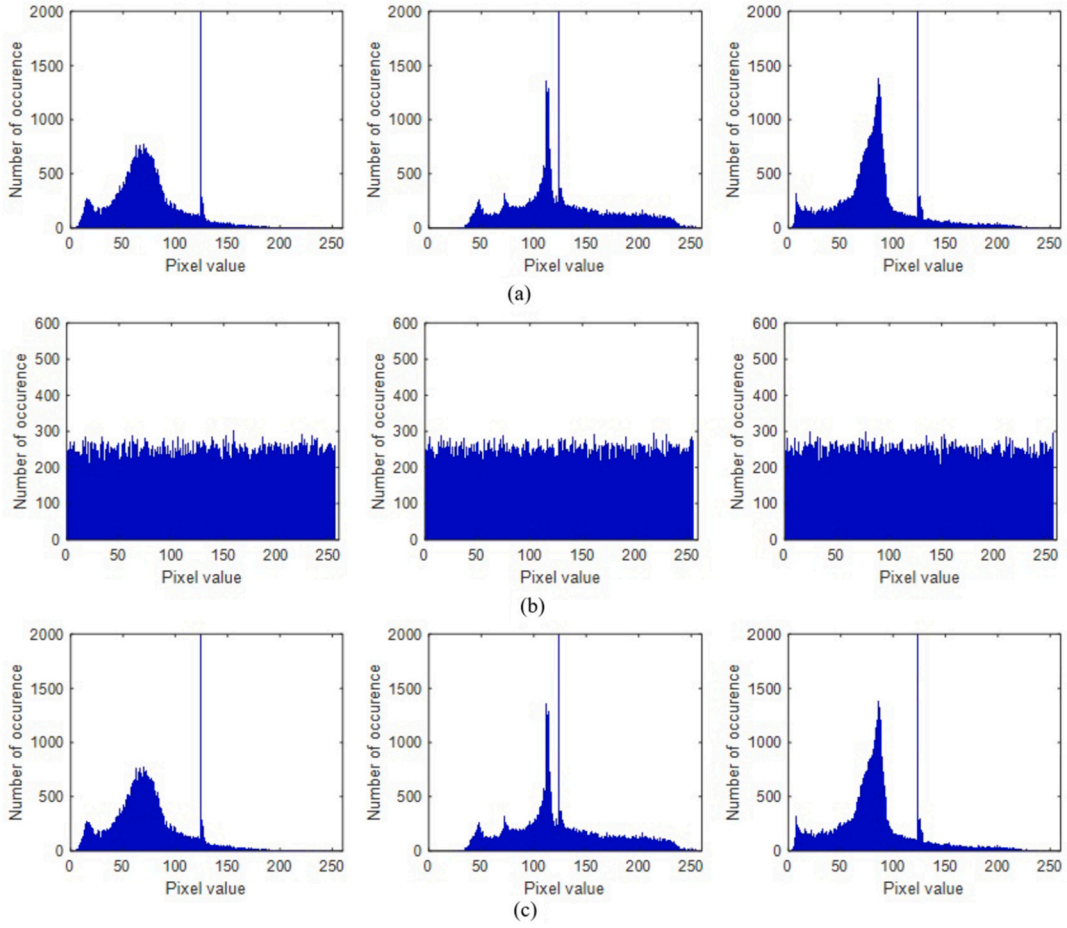

Fig. 9. Histogram of initial images (a), encoded images (b), and decoded images (c).

Table 4
Comparison between the results of this work and those developed in some recent studies.

		Image encryption algorithm				
	entropy	H	V	D	NPCR(%)	UACI(%)
Present algorithm	7.9972	-0.0019	-0.0008	-0.0045	99.6017	33.4922
Ref. [25]	7.9971	-0.0003	-0.0037	0.0020	99.59	33.27
Ref. [26]	7.9964	-0.0057	-0.0034	0.0073	99.6185	33.6245
Ref. [27]	7.9938	-0.0006	-0.0057	0.0009	99.60	34.63
Ref. [28]	7.9939	0.0015	-0.0090	-0.0120	99.54	34.25

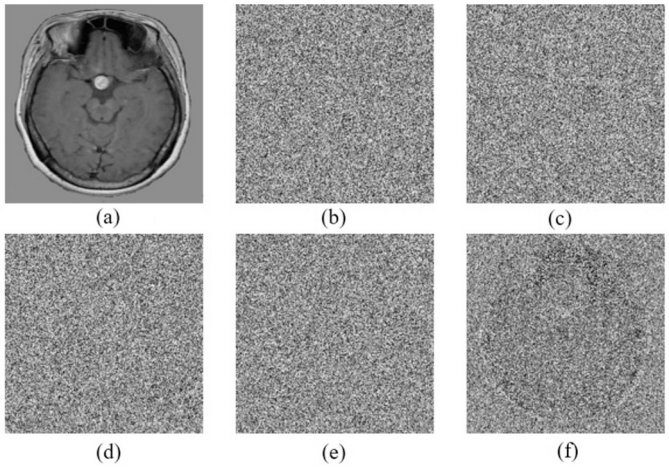

Fig. 10. Key sensitivity evaluation. (a) correct keys, (b) $a + 10^{-17}$, (c) $b + 10^{-17}$, (d) $x_0 + 10^{-17}$, (e) $y_0 + 10^{-17}$ and (f) $z_0 + 10^{-17}$.

where $\varepsilon_a, \varepsilon_b$ denote the estimated parameters of the system coefficients a, b respectively and $k_1, k_2, k_3 > 0$.

Substituting (17) into (16), we obtain the closed-loop system:

$$\begin{cases} \dot{x}_1 = [a - \varepsilon_a]x_3^3 - [a - \varepsilon_a]\mathrm{sgn}\left(x_2\right) - k_1 x_1, \\ \dot{x}_2 = -[b - \varepsilon_b] - k_2 x_2, \\ \dot{x}_3 = -k_3 x_3. \end{cases} \tag{18}$$

Accordingly, let us denote the error estimation of the parameters as follows:

$$\begin{cases} \varepsilon_1(t) = [a - \varepsilon_a(t)]; \\ \varepsilon_2(t) = [b - \varepsilon_b(t)]. \end{cases} \tag{19}$$

Based on Equation (19), the derivatives of the parameter estimation errors can be expressed as:

$$\begin{cases} \dot{\varepsilon_1} = -\dot{\varepsilon_a}, \\ \dot{\varepsilon_2} = -\dot{\varepsilon_b}. \end{cases} \tag{20}$$

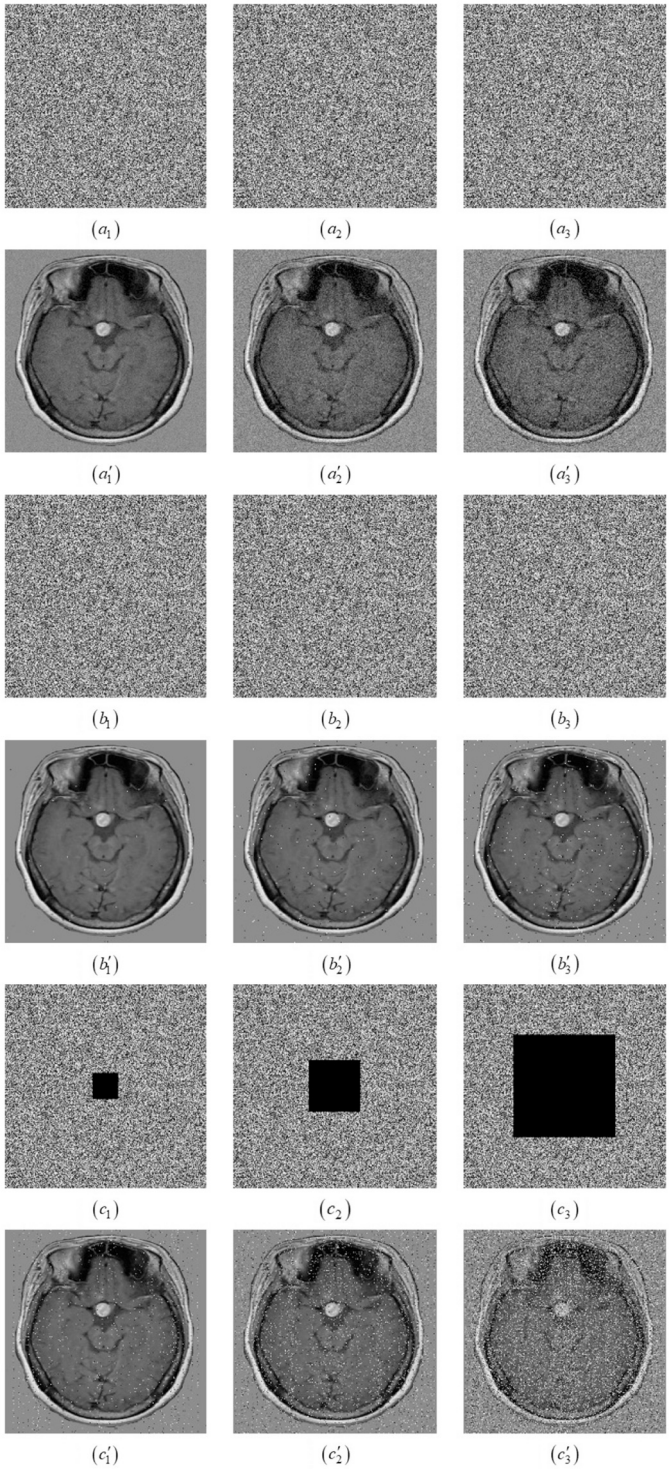

Fig. 11. Effects of noise and occlusion attacks. $(a_1)-(a_3)$ encoded with $0.001, 0.005$, and 0.01 Gaussian noise, respectively. $(a_1')-(a_3')$ corresponding decoded images. $(b_1)-(b_3)$ encoded images with $0.001, 0.005$, and 0.01 salt and pepper noise, respectively. $(b_1')-(b_3')$ corresponding decoded images. $(c_1)-(c_3)$ decoded image with $1/32, 1/16$, and $1/4$ loss respectively. $(c_1')-(c_3')$ corresponding decoded images.

Next, we reduce (18) to

$$\begin{cases} \dot{x}_1 = \varepsilon_1 x_3^3 - \varepsilon_1 \operatorname{sgn}(x_2) - k_1 x_1, \\ \dot{x}_2 = -\varepsilon_2 - k_2 x_2, \\ \dot{x}_3 = -k_3 x_3, \end{cases} \tag{21}$$

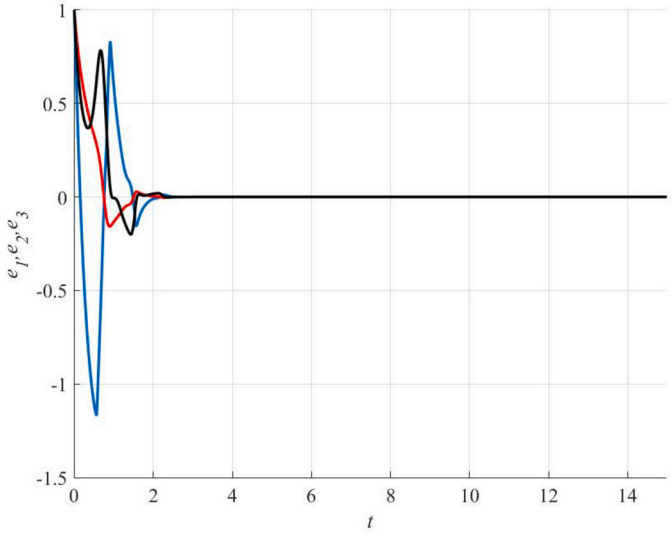

Fig. 12. Time series of anti-synchronization for error dynamical system (22) with controller (17).

Theorem 2. *If the controller is chosen as (17) and let the parameter's update laws are*

$$\begin{cases} \dot{\varepsilon_1}(t) = -x_1 x_3^3 + x_1 \operatorname{sgn}(x_2) - \eta(a - \varepsilon_a); \\ \dot{\varepsilon_2}(t) = b x_2 - \eta(b - \varepsilon_b), \end{cases} \tag{22}$$

then the synchronization between the driver system (17) and the response system (16) is approached if k_1, k_2, k_3 are positive constants.

Proof. We consider the Lyapunov function defined by

$$V(x_1, x_2, x_3, \varepsilon_1, \varepsilon_2) = \frac{1}{2}\left(x_1^2 + x_2^2 + x_3^2 + \varepsilon_1^2 + \varepsilon_2^2\right)$$

Differentiating the above function, we have

$$\dot{V}(x_1, x_2, x_3, \varepsilon_1, \varepsilon_2) =$$
$$= \left(x_1\dot{x_1} + x_2\dot{x_2} + x_3\dot{x_3} + \varepsilon_1\dot{\varepsilon_1} + \varepsilon_2\dot{\varepsilon_2}\right)$$

Taking time derivative of the above function along the trajectories of (22), we have

$$\dot{V} = -(k_1 x_1^2 + k_2 x_2^2 + k_3 x_3^2 + \eta\varepsilon_1^2 + \eta\varepsilon_2^2) \tag{23}$$

which is a negative function for $k_1, k_2, k_3 > 0$. Thus, due to the Lyapunov stability theory, we obtained that $\varepsilon_1(t) \to 0, \varepsilon_2(t) \to 0$ exponentially when $t \to \infty$.

The fourth order Runge-Kutta method is used to simulate numerically the introduced adaptive control system for system (16) with the adaptive control law (17) and the parameter update law (22). The parameters of system (1) are selected as $a = 3, b = 0.5$. In addition, we take the adaptive and update laws as $k_i = \eta_i = 2, (i = 1, \ldots, 3)$. Assume that the initial values of the estimated parameters are $(1, 1, 1)$ and the initial values of system (1) are taken as $(2, 3, 4)$. When the adaptive control law (22) and the parameter update law are used, the controlled system converges to the equilibrium $E = (0, 0, 0)$ exponentially as shown in Fig. 12.

7. Conclusions

A new three-dimensional chaotic oscillator with only nonlinear terms (three cubic functions and one signum function) is presented in this paper. The proposed oscillator displayed "hidden attractors" where no equilibrium points appeared. The bifurcation diagrams and Lyapunov exponents were investigated to determine the oscillator's dy-

namical characteristics. The comparison between the proposed biomedical image encryption algorithm with those of some recent algorithms shows a efficient and robust results. Moreover, the adaptive control of the new oscillator is given. We believe that the novelty and significance of our findings contribute to the field of nonlinear dynamics and its applications.

Declaration of competing interest

The authors have declared no conflict of interest.

Data availability

No data was used for the research described in the article.

Acknowledgements

This research is supported by Ajman University grant IRG 2023-24 /2.

References

[1] S. Cicek, U. Kocamaz, Y. Uyaroglu, Secure communication with a chaotic system owning, AEÜ, Int. J. Electron. Commun. 88 (2018) 52–62.
[2] H. Lin, C. Wang, W. Yao, Y. Tan, Chaotic dynamics in a neural network with different types of external stimuli, Commun. Nonlinear Sci. Numer. Simul. 90 (2020) 105390.
[3] A. Neamah, A. Shukur, A novel conservative chaotic system involved in hyperbolic functions and its application to design an efficient colour image encryption scheme, Symmetry 15 (2023) 1511.
[4] L. Wu, D. Wang, C. Zhang, A. Mohammadzadeh, Chaotic synchronization in mobile robots, Mathematics 10 (2022) 4568.
[5] Z. Tan, B. Hepburn, C. Tucker, M. Ali, Pattern recognition using chaotic neural networks, Discrete Dyn. Nat. Soc. 2 (1998) 243–247.
[6] A. Korolj, H. Wu, M. Radisic, A healthy dose of chaos: using fractal frameworks for engineering higher-fidelity biomedical systems, Biomaterials 219 (2019) 119363.
[7] E.N. Lorenz, Deterministic nonperiodic flow, J. Atmos. Sci. 20 (1963) 130–141.
[8] Z. Wei, Dynamical behaviors of a chaotic system with no equilibria, Phys. Lett. A 376 (2011) 102–108.
[9] S. Jafari, J. Sprott, S. Golpayegani, Elementary quadratic chaotic flows with no equilibria, Phys. Lett. A 377 (2013) 699–702.
[10] X. Wang, G. Chen, A chaotic system with only one stable equilibrium, Commun. Nonlinear Sci. Numer. Simul. 17 (2012) 1264–1272.
[11] S.K. Lao, Y. Shekofteh, S. Jafari, J. Sprott, Cost function based on Gaussian mixture model for parameter estimation of a chaotic circuit with a hidden attractor, Int. J. Bifurc. Chaos 24 (2014) 1450010.
[12] T. Kapitaniak, S. Mohammadi, S. Mekhilef, F. Alsaadi, T. Hayat, V. Pham, A new chaotic system with stable equilibrium: entropy analysis, parameter estimation, and circuit design, Entropy 20 (2018) 670.
[13] K. Rajagopal, A. Karthikeyan, A. Srinivasan, Bifurcation and chaos in time delayed fractional order chaotic oscillator and its sliding mode synchronization with uncertainties, Chaos Solitons Fractals 103 (2017) 347–356.
[14] V. Pham, S. Jafari, C. Volos, S. Vaidyanathan, T. Kapitaniak, A chaotic system with infinite equilibria located on a piecewise linear curve, Optik, Int. J. Light Electron Opt. 127 (2016) 9111–9117.
[15] S. Jafari, J. Sprott, Simple chaotic flows with a line equilibrium, Chaos Solitons Fractals 57 (2013) 79–84.
[16] K. Barati, S. Jafari, J. Sprott, V. Pham, Simple chaotic flows with a curve of equilibria, Int. J. Bifurc. Chaos 26 (2016) 1630034.
[17] M.F. Tolba, L.A. Said, A.H. Madian, A.G. Radwan, Fpga implementation of fractional-order integrator and differentiator based on Grunwald Letnikov's definition, in: 29th International Conference on Microelectronics (ICM), Beirut, 2017, pp. 1–4.
[18] S. Ismail, L. Said, A. Rezk, A. Radwan, A. Madian, M. Abu-Elyazeed, A. Soliman, Generalized fractional logistic map encryption system based on fpga, AEÜ, Int. J. Electron. Commun. 80 (2017) 114–126.
[19] G. Leonov, N. Kuznetsov, T. Mokaev, Hidden attractor and homoclinic orbit in Lorenz-like system describing convective fluid motion in rotating cavity, Commun. Nonlinear Sci. Numer. Simul. 28 (2015) 166–174.
[20] Y. Wang, A novel three dimension autonomous chaotic system with a quadratic exponential nonlinear term, Eng. Technol. Appl. Sci. Res. 2 (2012) 209–215.
[21] S.M. Seyedzadeh, S. Mirzakuchaki, A fast color image encryption algorithm based on coupled two-dimensional piecewise chaotic map, Signal Process. 92 (2012) 1202–1215.
[22] S. Zhu, C. Zhu, Image encryption algorithm with an avalanche effect based on a six-dimensional discrete chaotic system, Multimed. Tools Appl. 77 (2018) 29119–29142.
[23] T.G. Gao, Z.Q. Chen, A new image encryption algorithm based on hyper-chaos, Phys. Lett. A 372 (2008) 394–400.
[24] S. Behnis, A. Akhshani, S. Ahadpour, H. Mahnodi, A. Akhavan, A fast-chaotic encryption scheme based on piecewise nonlinear chaotic maps, Phys. Lett. A 366 (2007) 391–396.
[25] S. Maazouz, M. Toubal, A. Bengherbia, B. Houhou, O. Batel, Fpga implementation of a chaos-based image encryption algorithm, J. King Saud Univ, Comput. Inf. Sci. 34 (2022) 9926–9941.
[26] D. Dieu, N.J. Ruben, F.S.V. Nestor, T. Zeric, N.T. Jacques, Dynamic analysis of a novel chaotic system with no linear terms and use for dna-based image encryption, Multimed. Tools Appl. 23 (2020) 998–1014.
[27] G. Kaur, R. Agarwal, V. Patidar, Chaos based multiple order optical transform for 2d image encryption, Int. J. Eng. Sci. Technol. 23 (2020) 998–1014.
[28] X. Wang, M. Zhao, An image encryption algorithm based on hyperchaotic system and dna coding, Opt. Laser Technol. 143 (2021) 107316.
[29] D. Baleanu, S.S. Sajjadi, A. Jajarmi, O. Defterli, On a nonlinear dynamical system with both chaotic and non-chaotic behaviors: a new fractional analysis and control, Adv. Differ. Equ. 2021 (2021) 234.
[30] S.S. Sajjadi, D. Baleanu, A. Jajarmi, H.M. Pirouz, A new adaptive synchronization and hyperchaos control of a biological snap oscillator, Chaos Solitons Fractals 138 (2020) 109919.
[31] D. Baleanu, S.S. Sajjadi, J.H. Asad, A. Jajarmi, E. Estiri, Hyperchaotic behaviors, optimal control, and synchronization of a nonautonomous cardiac conduction system, Adv. Differ. Equ. 2012 (2021) 157.